Inorganic Chemistry

Article

Spectroscopic and Theoretical Study of a Mononuclear Manganese(III) Complex Exhibiting a Tetragonally Compressed Geometry

Quirin Scheifele,[†,‡] Christoph Riplinger,[§] Frank Neese,*,[§] Høgni Weihe,*,[||] Anne-Laure Barra,[⊥] Fanni Juranyi,[†] Andrei Podlesnyak,[†] and Philip L. W. Tregenna-Piggott*,[†]

Laboratory for Neutron Scattering, ETH Zürich and Paul Scherrer Institut, CH-5232 Villigen PSI, Switzerland, Department of Chemistry and Biochemistry, University of Bern, Freiestrasse 3, 3012 Bern, Switzerland, Institut für Physikalische und Theoretische Chemie, Universität Bonn, Wegelerstrasse 12, 53115 Bonn, Germany, Department of Chemistry, University of Copenhagen, Universitetsparken 5, DK-2100 Copenhagen, Denmark, and High Magnetic Field Laboratory, CNRS/MPI, B.P. 166, 38042 Grenoble, France

Inelastic neutron scattering and high-field electron paramagnetic resonance data are presented for [Mn(bpia)(OAc)(OCH$_3$)](PF$_6$), where bpia is bis(picolyl)(*N*-methylimidazole-2-yl)amine. Modeling of the data to the conventional fourth-order spin-Hamiltonian yielded the following parameters: $D = 3.526(3)$ cm^{-1}, $E = 0.588(6)$ cm^{-1}, $B_4^0 = -0.00084(7)$ cm^{-1}, $B_4^2 = -0.002(2)$ cm^{-1}, $B_4^4 = -0.0082(5)$ cm^{-1}, $g_x = 1.98(1)$, $g_y = 1.952(6)$, and $g_z = 1.978(5)$. The complex is of particular interest given the biochemical activity and the unusual stereochemistry distinguished by a rare example of a tetragonally compressed octahedron and a pronounced angular distortion imposed by the tetradentate tripodal bpia ligand. Ligand field, density functional theory, and complete active space self-consistent field ab initio calculations are presented that aim to relate the spectroscopic data to the molecular geometry.

1. Introduction

The sign of the zero-field-splitting (ZFS) parameter, D, in high-spin d^4 complexes is generally a reliable measure of the sign of the axial ligand field, being positive when the $^5A_{1g}$ (D_{4h}) term is lower-lying and negative when the $^5B_{1g}$ (D_{4h}) term is lower-lying. The correlation between the term splittings and the bond length changes resulting from the Jahn−Teller effect is well established when the octahedron is regular. Hence, a positive value of D is commonly regarded as a signature of an anomalous tetragonal compression of the octahedron.[1] The only exception so far reported is for *trans*-[Mn(cyclam)I$_2$]I, where it has been inferred that the energies of the components of the ground-state multiplet are dictated largely by mixing with low-lying charge-transfer states.[2] Manganese monomers[3] and clusters[4] are common throughout biology and are often more amenable to spectroscopic probes than to crystallographic determinations, particularly in the case of reaction intermediates or in situations where suitably diffracting crystals are elusive.[5] The ability to deduce the molecular structure then demands an appreciation of the extent to which the nature of the Jahn−Teller distortion can be inferred in complexes where the angular distortion of the first coordination sphere is considerable.

* To whom correspondence should be addressed. E-mail: neese@thch.uni-bonn.de (F.N.), weihe@kiku.dk (H.W.), philip.tregenna@psi.ch (P.L.W.T-P.). Fax: +41 56 310 2939.

† ETH Zürich and Paul Scherrer Institut.

‡ University of Bern.

§ Universität Bonn.

|| University of Copenhagen.

⊥ High Magnetic Field Laboratory, CNRS/MPI.

(1) Griffith, J. S. *The Theory of Transition Metal Ions*; Cambridge University Press: London, 1961. Griffith, J. S. *Trans. Faraday Soc.* **1960**, *56*, 193. Abragam, A. Bleaney, B. *Electron Paramagnetic Resonance of Transition Ions*; Oxford University Press: London, 1970. Bencini, A. Ciofini, I. Uytterhoeven, M. G. *Inorg. Chim. Acta* **1998**, *274*, 90.

(2) Mossin, S.; Weihe, H.; Barra, A-L. *J. Am. Chem. Soc.* **2002**, *124*, 8764.

(3) Yamakura, F.; Kobayashi, K.; Ue, H.; Konno, M. *Eur. J. Biochem.* **1995**, *227*, 700−706. Renault J. P.; Verchere-Beaur C.; Morgenstern-Badarau, I.; Yamakura, F.; Gerloch, M. *Inorg. Chem.* **2000**, *39*, 2666−2675. Zhang, W.; Loebach, J. L.; Wilson, S. R.; Jacobsen, E. N. *J. Am. Chem. Soc.* **1990**, *112*, 2801−2803. Lai, T.-S.; Che, C.-M.; Kwong, H.-L.; Peng, S.-M. *J. Chem. Soc., Chem. Commun.* **1997**, 2373−2374.

(4) Ferreira, K. N.; Iverson, T. M.; Maghlaoui, K.; Barber, J.; Iwata, S. *Science* **2004**, *303*, 1831−1838. Wilce, M. C. J.; Bond, C. S.; Dixon, N. E.; Freeman, H. C.; Guss, J. M.; Lilley, P. E.; Wilce, J. A. *Proc. Natl. Acad. Sci. U.S.A.* **1998**, *95*, 3472−7. Bewley, M. C.; Jeffrey, P. D.; Patchett, M. L.; Kanyo, Z. F.; Baker, E. N. *Structure* **1999**, *7*, 435.

(5) *Physical Methods in Bioinorganic Chemistry: Spectroscopy and Magnetism*; Que, L., Jr., Ed.; University Science Books: Sausalito, CA, 2000.
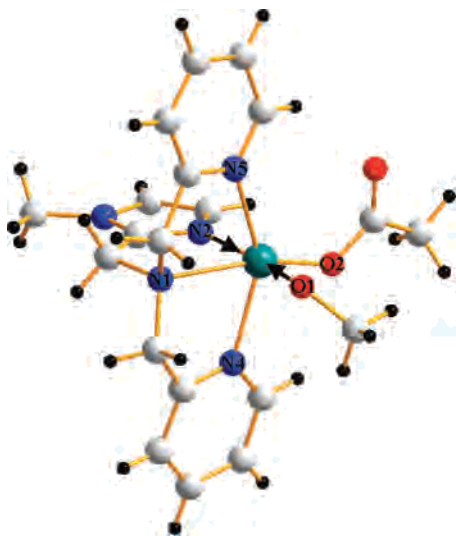
Figure 1. Structure of [Mn(bpia)(OAc)(OCH₃)](PF₆). The manganese−ligand bond lengths are indicative of a compression of the octahedron along the Mn−N2 and Mn−O1 bonds, as indicated in the figure.

Table 1. Bond Distances and Angles Defining the First Coordination Sphere about Manganese in [Mn(bpia)(OAc)(OCH₃)](PF₆)[6]

bond lengths/Å		bond angles/deg	
Mn−O(1)	1.777(3)	O(1)−Mn−O(2)	99.2(1)
Mn−O(2)	1.955(3)	O(1)−Mn−N(2)	171.4(1)
Mn−N(1)	2.286(3)	O(2)−Mn−N(1)	160.4(1)
Mn−N(2)	2.014(3)	N(1)−Mn−N(2)	79.2(1)
Mn−N(4)	2.243(3)	N(1)−Mn−N(4)	74.1(1)
Mn−N(5)	2.218(3)	N(1)−Mn−N(5)	74.6(1)

A series of manganese(III) compounds that catalyze the oxidation of 3,5-di-*tert*-butylcatechol to 3,5-di-*tert*-butylquinone efficiently has recently been reported.[6] Our interest in these compounds lies in the strong geometric constraints imposed by the chelating ligand and the consequent effect on the ground-state spin-Hamiltonian parameters. The compound chosen for detailed study is [Mn(bpia)(OAc)(OCH₃)]-(PF₆), where bpia is bis(picolyl)(*N*-methylimidazole-2-yl)-amine. The coordination about the manganese(III) cation deviates radically from a perfect octahedron both in terms of the heteroleptic coordination sphere and in the bond angles imposed by the chelating bpia ligand, as seen in Figure 1 and documented in Table 1. The experimental techniques employed to study this system are high-field multifrequency electron paramagnetic resonance (HFEPR) and inelastic neutron scattering (INS). This study marks the first use of INS to elucidate the electronic structure of a catalytically active system. It is shown below that the combination of the two techniques enables the determination of the ground-state spin-Hamiltonian parameters to excellent precision. The pronounced angular distortion and heteroleptic coordination sphere provides a theoretical challenge that goes far beyond the homoleptic manganese(III) complexes that have hitherto been considered.[7−9] The ZFS parameters of the complex are calculated using a variety of theoretical methods and compared to the experimental values. Consequently, we are able to provide a critical assessment of the extent to which the electronic and molecular structure may be interrelated in bioinorganic manganese(III) complexes by the state-of-the-art techniques currently available.

2. Experimental Section

2.1. Syntheses. All syntheses were carried out with chemicals of natural isotopic abundance. The ligand bpia (bis[(2-pyridiyl)-methyl]-[(1-methylimidazol-2-yl)methyl]amine also known as bis-(picolyl)-[(*N*-methylimidazol-2-yl)amine) was synthesized from 2-(chloromethyl)-1-methylimidazole (chloride salt), bis(picolyl)-amine, and triethylamine as previously described.[10] A modification to the synthesis of the preliminary product (1-methylimidazol-2-yl)methanol was made, as described in refs 11 and 12

[Mn(bpia)(OAc)(OCH₃)][PF₆]. Following the method described by Triller et al.,[6] equimolar amounts of bpia (3.00 g, 10.24 mol) and Mn(OAc)₃·2H₂O (2.75 g, 10.24 mol) were allowed to react in 1 L of methanol in the presence of acetic acid (7.15 mL). The resulting green solution was stirred for 30 min and filtered. [Bu₄N]-[PF₆] (3.97 g, 10.24 mol) was added, and the reaction mixture was stirred for another 30 min. The precipitated fine-green crystalline powder was collected by filtration, washed first with ice-cold methanol and then diethylether, and dried for 90 min at 100 °C. The mother liquor was then collected, 1 L of diethylether was added, and the mixture was placed in a refrigerator. Further crystals that formed overnight were collected, washed with ice-cold methanol and diethylether, and dried for 90 min at 100 °C. The two crops were combined once their purity had been verified (8.26 g, 0.014 mol, 68%). Mp: 223−247 °C. HCN analysis results, Anal. Calcd for C₂₀H₂₅N₅F₆MnO₃P: C, 41.18; H, 4.32; N, 12.01. Found: C, 41.46; H, 4.32; N, 11.33.

2.2. Inelastic Neutron Scattering Measurements. The INS measurements were carried out on FOCUS, a direct geometry time-of-flight spectrometer for cold neutrons at SINQ, Paul Scherrer Institut (PSI), Villigen, Switzerland, with detector banks spanning 9.64° to 129.4° in the scattering plane.[13] For a series of measurements at 1.5, 6, 15, and 30 K, a wavelength of $\lambda = 4.85$ Å was chosen, yielding an energy transfer window up to ∼20.5 cm⁻¹ and a resolution of ∼1 cm⁻¹ at the elastic peak. An additional measurement at 6 K was carried out; choosing a wavelength of 5.85 Å afforded an improved resolution of 0.4 cm⁻¹ at the elastic peak but at the cost of a reduced energy window extending to ∼7 cm⁻¹ on the neutron-energy-loss side of the spectrum. Approximately 3 g of [Mn(bpia)(OAc)(OCH₃)][PF₆] was loaded in a 10 mm diameter double-well hollow aluminum measurement cylinder, sealed under a He atmosphere, and placed in a standard ILL Orange cryostat. An empty aluminum can of the same dimension as the sample holder was measured, and the spectrum

(6) Triller, M. U.; Pursche, D.; Hsieh, W.; Pecoraro, V. L.; Rompel, A.; Krebs, B. *Inorg. Chem.* **2003**, *42*, 6274−6283.

(7) Barra, A.-L.; Gatteschi, D.; Sessoli, R.; Abbati, G. L.; Cornia, A.; Fabretti, A. C.; Uytterhoeven, M. G. *Angew. Chem.* **1997**, *109*, 2423−2426. Barra, A.-L.; Gatteschi, D.; Sessoli, R.; Abbati, G. L.; Cornia, A.; Fabretti, A. C.; Uytterhoeven, M. G. *Angew. Chem., Int. Ed. Engl.* **1997**, *36*, 2329−2331.

(8) Krzystek, J.; Yeagle, G. J.; Park, J.-H.; Britt, R. D.; Meisel, M. W.; Brunel, L.-C.; Telser, J. *Inorg. Chem.* **2003**, *42*, 4610.

(9) Tregenna-Piggott, P. L. W.; Weihe, H.; Barra, A.-L. *Inorg. Chem.* **2003**, *42*, 8504.

(10) Wei, N.; Murthy, N. N.; Tyeklár, Z.; Karlin, K. D. *Inorg. Chem.* **1994**, *33*, 1177−1183.

(11) Pascaly, M.; Duda, M.; Rompel, A.; Sift, B. H.; Meyer-Klaucke, W.; Krebs, B. *Inorg. Chim. Acta* **1999**, *291*, 289−299.

(12) Reese, C. B.; Pei-Zhuo, Z. *J. Chem. Soc., Perkin Trans.* **1993**, *1*, 2291−2301.

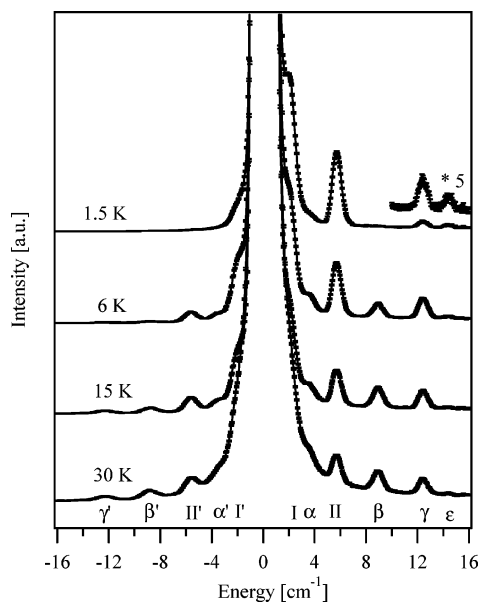(13) Mesot, J.; Janssen, S.; Holitzner, L.; Hempelmann, R. *J. Neutron Res.* **1996**, *3*, 293.

Figure 2. INS spectra of [Mn(bpia)(OAc)(OCH$_3$)][PF$_6$] measured at 4.85 Å between 1.5 and 30 K, summed over all detectors. The transition-labeling scheme follows Figure 4.

value was subtracted from that of the sample. The detector efficiency correction was performed using data collected from vanadium. The data were reduced and analyzed using the *DAVE*[14] (Data Analysis and Visualisation Environment) program package, written specifically for the reduction and analysis of neutron scattering data.

2.3. High-Field EPR (HFEPR) Measurements. HFEPR measurements were carried out using apparatus at the Grenoble High Magnetic Field Laboratory, described in detail previously.[15] The sample was finely ground and pressed into a pellet to avoid preferential orientation of the crystallites in the strong magnetic field. The pellet was wrapped in Teflon tape and placed in a cryostat, affording a stable temperature environment between 5 and 20 K. Gun diodes operating at 95 and 115 GHz equipped with a second-, third-, fourth-, and fifth-harmonic generator were used as the radiation source. The sample was subject to an external magnetic field varying between 0 and 11 T, provided by a superconducting magnet.

3. Results

The low-lying eigenstates of the title compound were characterized by INS and EPR. While both techniques have their own virtue, the all-important ZFS of the ground-state manifold is immediately apparent from inspection of the INS spectra; hence, it is natural to begin by discussing the INS data.

Figures 2 and 3 show the INS spectra of [Mn(bpia)(OAc)-(OCH$_3$)][PF$_6$], as a function of temperature and neutron

(14) Azuah, R.; Copley, J.; Dimeo, R.; Park, S.; Lee, S.-H.; Munter, A.; Kneller, L.; Qiu Y.; Peral, I.; Brown, C.; Kienzle, P.; Tregenna-Piggott, P. L.W. *DAVE*, 1.4 beta version; NIST Center for Neutron Research, U.S. National Institute of Standards and Technology: Gaithersburg, MD. http://www.ncnr.nist.gov/dave.

(15) Muller, F.; Hopkins, A.; Coron, N.; Grynberg, M.; Brunel, L.-C.; Martinez, G. *Rev. Sci. Instrum.* **1989**, *60*, 3681. Barra, A.-L.; Brunel, L.-C.; Robert, J. B. *Chem. Phys. Lett.* **1990**, *165*, 107.

(16) Basler, R.; Tregenna-Piggott, P. L. W.; Andres, H.-P.; Dobe, C.; Gudel, H.-U.; Janssen, S.; McIntyre, G. J. *J. Am. Chem. Soc.* **2001**, *123*, 3377−3378.

Figure 3. INS spectra of [Mn(bpia)(OAc)(OCH$_3$)][PF$_6$] collected at 5.85 Å and 6 K. The transition-labeling scheme follows Figure 4.

Table 2. Experimentally Observed INS Transition Energies of [Mn(bpia)(OAc)(OCH$_3$)][PF$_6$]

transition	energy (cm^{-1})	temperature and wavelength
γ'	-12.340 ± 0.018	30 K[a]
β'	-8.858 ± 0.010	30 K[a]
II$'$	-5.623 ± 0.009	30 K[a]
α'	-3.542 ± 0.068	6 K[b]
I$'$	-2.013 ± 0.005	6 K[b]
I	2.120 ± 0.003	6 K[b]
α	3.662 ± 0.017	6 K[b]
II	5.705 ± 0.001	6 K[a]
β	8.917 ± 0.005	6 K[a]
γ	12.420 ± 0.004	6 K[a]
ϵ	14.42 ± 0.03	1.5 K[a]

[a] 4.85 Å. [b] 5.85 Å.
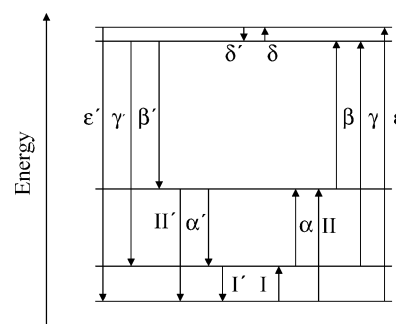
Figure 4. Energy-level diagram depicting the observed INS transitions for [Mn(bpia)(OAc)(OCH$_3$)][PF$_6$]. The labeling scheme follows ref 16.

incident wavelength. The spectra should serve to dispel the myth that INS is confined to samples absent of hydrogen. Transitions between the states of the ground multiplet of manganese(III) occur in an energy range not strongly affected by the incoherent scattering due to hydrogen. The INS technique may therefore be readily employed in the study of bioinorganic manganese(III) systems.

At 1.5 and 6 K, the spectrum is dominated by two intense peaks at 2.120 ± 0.003 and 5.705 ± 0.001 cm^{-1}, clearly visible in the higher-resolution spectrum displayed in Figure 3. The spectrum changes markedly on change of temperature, with prominent hot bands appearing at 8.917 ± 0.005 and 12.420 ± 0.004 cm^{-1}. The observed transitions are listed in Table 2, from which the energy-level diagram in Figure 4 was constructed.

Table 3. Energies, Wavefunctions, and INS Transition Probabilities within the $S = 2$ Manifold, Resulting from Treating the Rhombic ZFS Term as a Perturbation to the States Resulting from the Axial ZFS Term (eq 1)[a]

zeroth-order wavefunctions	zeroth-order energies	first-order corrected wavefunctions	second-order corrected energy	INS transition probabilities from state $\lvert a'\rangle$	INS transition probabilities from state $\lvert e'\rangle$
$\lvert a\rangle \equiv \lvert 0\rangle$	$-2D$	$\lvert a'\rangle = \lvert a\rangle + \dfrac{\sqrt{3}}{2}\dfrac{E}{D}\lvert e\rangle$	$-2D - {}^{3}\!/_{4}(E/D)^2$		${}^{1}\!/_{2}(E/D)^2$
$\lvert b\rangle \equiv \dfrac{1}{\sqrt{2}}(\lvert 1\rangle - \lvert -1\rangle)$	$-D$	$\lvert b'\rangle = \lvert b\rangle$	$-D - 3E$	~ 2	$\sim {}^{4}\!/_{3}$
$\lvert c\rangle \equiv \dfrac{1}{\sqrt{2}}(\lvert 1\rangle + \lvert -1\rangle)$	$-D$	$\lvert c'\rangle = \lvert c\rangle$	$-D + 3E$	~ 2	$\sim {}^{4}\!/_{3}$
$\lvert d\rangle \equiv \dfrac{1}{\sqrt{2}}(\lvert 2\rangle - \lvert -2\rangle)$	$2D$	$\lvert d'\rangle = \lvert d\rangle$	$2D$	0	$\sim {}^{8}\!/_{3}$
$\lvert e\rangle \equiv \dfrac{1}{\sqrt{2}}(\lvert 2\rangle + \lvert -2\rangle)$	$2D$	$\lvert e'\rangle = \lvert e\rangle - \dfrac{\sqrt{3}}{2}\dfrac{E}{D}\lvert a\rangle$	$2D + {}^{3}\!/_{4}(E/D)^2$	${}^{1}\!/_{2}(E/D)^2$	

[a] The zeroth-order wavefunctions are given in terms of the M_s quantum number. The transition probabilities are those between the first-order corrected wavefunctions and were calculated according to eq 2.

We now proceed to rationalize the energies and intensities of INS peaks within the framework of the $S = 2$ spin Hamiltonian,

$$\hat{H}_\mathrm{s} = D[\hat{S}_z^2 - ({}^1\!/_3)S(S + 1)] + E[\hat{S}_x^2 - \hat{S}_y^2] \qquad (1)$$

commonly applied to describe EPR spectra of manganese-(III) complexes.[9] In the limit where the magnitude of E/D is small, the rhombic term in eq 1 may be considered as a perturbation to the axial term. It is convenient to describe the INS spectrum within this approximation, as the energies and wavefunctions then have a simple form. They are given in Table 3, along with the INS transition probabilities, calculated from the expression[17]

$$\mathrm{INS}_\mathrm{TP} \propto \frac{1}{3}(2\lvert\langle\Psi_f\lvert\hat{S}_z\lvert\Psi_i\rangle\rvert^2 + \lvert\langle\Psi_f\lvert\hat{S}_+\lvert\Psi_i\rangle\rvert^2 + \lvert\langle\Psi_f\lvert\hat{S}_-\lvert\Psi_i\rangle\rvert^2) \qquad (2)$$

When D is positive, the ground state is $\lvert a'\rangle$; two cold transitions at energies $D + {}^{3}\!/_{4}(E/D)^2 - 3E$ and $D + {}^{3}\!/_{4}(E/D)^2 + 3E$ to states $\lvert b'\rangle$ and $\lvert c'\rangle$, respectively. Should D be negative, $\lvert e'\rangle$ constitutes the ground state; two strong transitions are also expected with the same splitting but at $\sim 2D$ higher energy. From the 1.5 K spectrum alone, therefore, we may immediately conclude that either D is moderate in magnitude and positive or rather small and negative. Either way, the energy difference between the transitions is a direct measure of the parameter E, the difference being $6E$. The temperature dependence of the spectrum provides unambiguous confirmation that D is indeed positive. Fitting the eigenvalues of eq 1 to the observed transition energies given in Table 2 results in the ZFS parameters: $D = 3.5140(7)$ and $E = 0.6213(3)$ cm^{-1}. Figure 5 shows theoretical INS spectra calculated at 15 K,

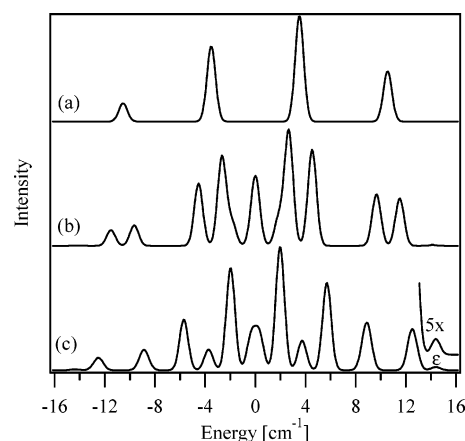**Figure 5.** Theoretical INS spectra calculated at 15 K from a $S = 2$ spin system with D set to 3.5140 cm^{-1} and E set to (a) 0, (b) 0.31065, and (c) 0.6213 cm^{-1}.

with $D = 3.5140$ cm^{-1} and values for E of 0, 0.31065, and 0.6213 cm^{-1}. The eigenvalues and eigenfunctions were calculated by exact numerical diagonalization of eq 1, and the intensities calculated according to eq 2. Of particular interest is the transition labeled ϵ, which is seen to grow in intensity upon increasing E. Transition ϵ occurs between states $\lvert a'\rangle$ and $\lvert e'\rangle$ with an intensity approximately proportional to $(E/D)^2$. This transition has never been observed before but is clearly visible in the experimental spectra of [Mn(bpia)(OAc)(OCH$_3$)][PF$_6$], reflecting the strong rhombic distortion in this system. The energies and relative intensities of the bands in the theoretical spectrum shown in Figure 5c correspond very well with the 15 K experimental spectrum, providing confidence in the validity of the model parameters.

The EPR experiments allow the g values to be determined. Furthermore, recording the spectra at different excitation frequencies enables many transitions to be documented, which may be considered as unique observations if the difference in the excitation frequencies is comparable to the ZFS. In total, 33 resonances were documented from spectra recorded between 5 and 30 K at excitation frequencies of 95, 230, 285, 345, and 460 GHz. The resonances were assigned to transitions between the levels of the $S = 2$ ground state with the external magnetic field aligned along the z, x,

(17) Since the INS bands occur at different energies but result from the counts collected in detectors at fixed angular positions, each band samples a different range of values of the momentum transfer vector Q. Strictly, this should be taken into consideration when simulating the spectra. However, the observed bands cover an energy transfer range small enough for this contribution to be neglected. Furthermore, the dependence of the intensity on the Q vector is largely washed-out due to multiple scattering, this itself being a consequence of the high proton concentration.

Table 4. Experimentally Determined Values of the Spin-Hamiltonian Obtained from Least-Square Refinement of the Eigenvalues of Eq 3 to the 39 Observations Obtained from INS and EPR Experiments

parameter	value and error	parameter	value and error
D	3.526(3) cm^{-1}	g_x	1.98(1)
E	0.588(6) cm^{-1}	g_y	1.952(6)
B_4^0	−0.00084(7) cm^{-1}	g_z	1.978(5)
B_4^2	−0.002(2) cm^{-1}		
B_4^4	−0.0082(5) cm^{-1}		

or *y* axes. In previous works, we have adopted a procedure whereby the spin-Hamiltonian parameters are derived by fitting the eigenvalues to the observed EPR resonance fields.[9] The methodology is extended in this study to refine on the INS and EPR observations simultaneously.[18] Given the large number of observed spectral features, the spin-Hamiltonian is extended to include fourth-order terms. Refining the eigenvalues of the Hamiltonian,

$$\hat{H}_s = D\left[\hat{S}_z^2 - \frac{1}{3}S(S+1)\right] + E[\hat{S}_x^2 - \hat{S}_y^2] +$$

$$B_4^4\frac{1}{2}[\hat{S}_+^4 + \hat{S}_-^4] + B_4^0[35\hat{S}_z^4 - 155\hat{S}_z^2 + 72] +$$

$$B_4^2\frac{1}{4}[(7\hat{S}_z^2 - 11)(\hat{S}_+^2 + \hat{S}_-^2) + (\hat{S}_+^2 + \hat{S}_-^2)(7\hat{S}_z^2 - 11)] +$$

$$\mu_B(g_x B_x \hat{S}_x + g_y B_y \hat{S}_y + g_z B_z \hat{S}_z) \qquad (3)$$

to 39 observations results in the parameters documented in Table 4. The second-order ZFS parameters change little from those derived from the INS data alone, with the fourth-order terms barely significant. The *g* values exhibit a high degree of anisotropy consistent with the large *E/D* ratio. An excellent reproduction of the INS and EPR data is afforded from these parameters, as shown in Figure 6 where a representative EPR spectrum is displayed alongside the corresponding simulation. Upon warming to 280 K, the INS peaks and EPR resonances broaden but no change in the peak positions was discerned, suggesting that the coordination sphere about the manganese(III) cation is rigid in the 1.5 to 280 K temperature range.

4. Theoretical Analysis

4.1. Angular Overlap Model (AOM) Calculations. The AOM is a natural choice for inter-relating single ion anisotropy with geometrical distortions, having been employed to great effect in previous works on manganese(III) complexes.[7−9] However, the heteroleptic [Mn(bpia)(OAc)-(OCH$_3$)]$^+$ complex presents a severe limitation as to what can be sensibly extracted from an AOM calculation. Any attempt to fit the ground-state spin-Hamiltonian parameters of [Mn(bpia)(OAc)(OCH$_3$)]$^+$ within the framework of the AOM would be a pointless exercise as the multitude of bonding parameters so obtained would be of no chemical value. Nevertheless, it is an instructive exercise to consider the effect of the angular distortion imposed by the tripodal
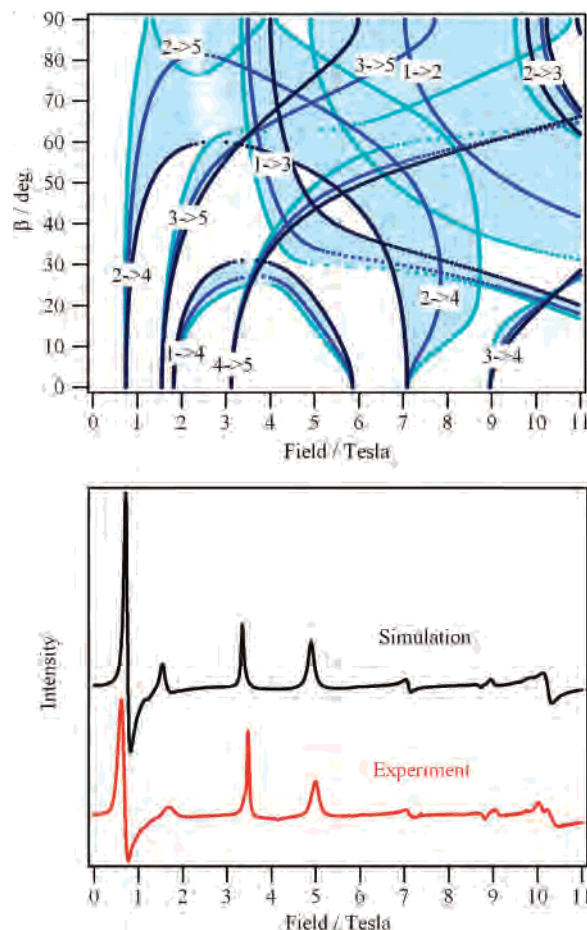
(18) Høgni, W. *SIM*; University of Copenhagen. Glerup, J.; Weihe, H. *Acta Chem. Scand.* **1991**, *45*, 444.

Figure 6. (upper) Angular dependence of the resonances. The dark blue and light blue lines refer to the *xz* and *yz* planes, respectively, with the navy blue lines intermediate. The ordinate is the angle between the magnetic field and the molecular *z* axis. A necessary condition for a line to appear in the powder spectrum is first a nonzero transition probability for the corresponding transition as well as a vertical tangent in the corresponding angular dependence curve. (lower) Experimental and simulated powder EPR spectra of [Mn(bpia)(OAc)(OCH$_3$)][PF$_6$] at 5 K and 345 GHz.

ligand on the ground-state spin-Hamiltonian parameters of an idealized complex.

At first sight, the complex displayed in Figure 1 is an ugly looking beast exhibiting no sign of symmetry. However, the bioinorganic flavor masks an underlying simplicity. The effect of the tripodal ligand is essentially to reduce the N(1)−Mn−N(X) (X = 2,3,5) bond angle from 90° to values in the range of ∼75−79°. It is a trivial matter to calculate the change in the energy levels along this coordinate using the AOM. A complex based upon [Mn(bpia)(OAc)(OCH$_3$)]$^+$ is constructed in which the manganese(III) ion is coordinated by six linear ligators that differ in their bonding descriptions only on account of their different bond distances.

The AOM parameters are broadly based upon those previously determined for the [Mn(OH$_2$)$_6$]$^{3+}$ cation,[9] which is tetragonally elongated.[19] By assuming that the e_σ and e_π parameters vary as a function of bond distance *r*, according to $1/r^5$ and $1/r^6$, respectively,[9] the bonding parameters for a

(19) Tregenna-Piggott, P. L. W.; Andres, H. P.; McIntyre, G. J.; Best, S. P.; Wilson, C. C.; Cowan, J. A. *Inorg. Chem.* **2003**, *42*, 1350.
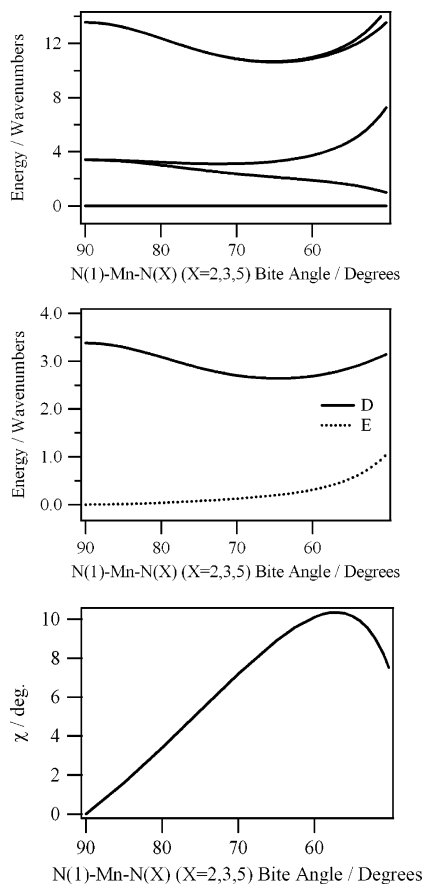
Figure 7. (upper) Walsh diagram showing the energies of the five lowest-lying states of a manganese(III) complex resembling [Mn(bpia)(OAc)-(OCH₃)](PF₆), as a function of the N(1)−Mn−N(X) (X = 2,3,5) bite angle. (middle) Corresponding values of the ZFS parameters. (lower) Angle χ defining the orientation of the principal value of the $\boldsymbol{D}$ tensor relative to the Mn1−O1 bond vector. The principal value of the $\boldsymbol{D}$ tensor bisects the Mn1−O1 and Mn−N1 bond vectors. With the bite angle set to 90°, the first coordination sphere is rigidly octahedral. The ligand field calculation was undertaken with B = 760, C = 3290, and ζ = 281 cm⁻¹ and the following parameters. Ligands N(2) and O(1): e_σ = 9433 cm⁻¹, e_π = 707 cm⁻¹; N(1), N(4), N(5), and O(2), e_σ = 4232 cm⁻¹, e_π = 381 cm⁻¹. Further details are provided in the text.

tetragonally compressed octahedron, with bond distances broadly based upon those determined for the [Mn(bpia)-(OAc)(OCH₃)]⁺ complex, are calculated as follows: ligands N(2) and O(1), e_σ = 9433 cm⁻¹, e_π = 707 cm⁻¹; N(1), N(4), N(5), and O(2), e_σ = 4232 cm⁻¹, e_π = 381 cm⁻¹. We emphasize that the ligands are forced to be linearly ligating, in contrast to the manganese(III)−water interaction where the sizable value for the E/D ratio has been attributed to the π anisotropy.[9]

With the use of these parameters, the Walsh diagram displayed in the upper part of Figure 7 was constructed, calculated in zero magnetic field using the *LIGFIELD* program, developed by Jesper Bendix.[20] Next, the calculation was repeated for 216 independent values for the magnetic field and the energies of the ground-state manifold modeled by the eigenvalues of the S = 2 spin-Hamiltonian,

$$\hat{H}_s = SDS + \beta BgS \qquad (4)$$

(20) Bendix, J. *Comp. Coord. Chem. II* **2004**, *2*, 673−676.

Least-squares refinement of the eigenvalues of eq 4 to the five lowest-lying eigenvalues of the AOM calculations yielded the $\boldsymbol{D}$ tensor and g matrix in the reference coordination frame. The principal values were determined via the transformations

$$U_D{}^{-1}DU_D = D'; \quad U_g{}^{-1}gU_g = g' \qquad (5)$$

where D' and g' refer to the $\boldsymbol{D}$ tensor and $\boldsymbol{g}$ matrix in coordinate frames in which they are diagonal. The matrices U_D and U_g contain the direction cosines relating the two coordinate systems, from which the Euler angles can be calculated. The middle section of Figure 7 shows the values of the ZFS parameters D and E, derived from the principal values of the $\boldsymbol{D}$ tensor. The angle between the principal value of the $\boldsymbol{D}$ tensor and the Mn1−O1 bond vector is displayed in the lower section of the plot.

When the N(1)−Mn−N(X) (X = 2,3,5) bite angle is set to 90°, the calculated eigenvalues reflect a compressed octahedral structure exhibiting axial symmetry. The effect of the angular distortion is to reduce the strength of the axial field while introducing anisotropy in the equatorial plane. With the bite angle set to 77°, the distribution of the low-lying states is still indicative of a tetragonally compressed octahedron, with D positive, in accordance with our spectroscopic measurements. The calculated value of E/D is a meagre 0.020, increasing to 0.055 when repeated using the actual angular coordinates of the [Mn(bpia)(OAc)(OCH₃)]⁺ complex but still well short of the value of 0.18 observed experimentally. Though the σ-donor capacities of the ligands are not expected to differ drastically, the spin-Hamiltonian parameters of the complex cannot be explained without due consideration of the heteroleptic coordination. The correlation between the sign of D and the nature of the Jahn−Teller distortion still holds for bite angles down to ~50°, below which the very notion of compressed/elongated octahedra is inappropriate. Interest in the dependence of the orientation of the $\boldsymbol{D}$ tensor on the bite angle stems from work on derivatives of the single molecule magnet Mn12, as the orientation of the $\boldsymbol{D}$ tensors of the constituent manganese-(III) centers, relative to that of the cluster, largely determines the signs and magnitudes of the higher-order ZFS terms responsible for quantum tunneling processes.[21] With the bite angle set to 90°, the $\boldsymbol{D}$ tensor is axially symmetric with the principal direction aligned along the Mn−O1 bond vector. The angular distortion breaks the symmetry of the $\boldsymbol{D}$ tensor, with the hard axis closely aligned along the Mn−N1 bond vector. Decreasing the bite angle from 90° to 50° is predicted to give rise to a pronounced rotation of the $\boldsymbol{D}$ tensor about an axis perpendicular to the N1−Mn−O1 plane, but the magnitude of the rotation is predicted to have a distinctly nonlinear dependence upon the bite angle in the region where the anisotropy is appreciable, this being concomitant with a general increase in the ZFS of the ground state.

4.2. ab Initio and Density Functional Theory (DFT) Calculations. Calculations were performed with the *ORCA*

(21) Barra, A.-L.; Caneschi, A.; Cornia, A.; Gatteschi, D.; Gorini, L.; Heiniger, L.-P.; Sessoli, R.; Sorace, L. *J. Am. Chem. Soc.* **2007**, *129*, 10754−10762.

program,[22] employing the TZVP basis set.[23] The complete active space self-consistent field (CASSCF) calculations were converged for the average of the five quintet states that arise from the d^4 configuration at the Mn(III) center. The spin−orbit coupling (SOC) was represented by the spin−orbit mean-field (SOMF) approximation[24] in the implementation of ref 25. The SOMF approximation is believed to represent accurately the full Breit−Pauli SOC operator and explicitly incorporates the spin-same orbit (SSO) and spin-other orbit (SOO) interactions.

Three different structures were tested: (a) the experimental structure, (b) a structure that was optimized at the RI[26]-BP86[27]/TZVP level, and (c) an optimized structure in which only the positions of the hydrogen atoms were relaxed.

For the DFT models, two different approximations to the SOC term were tested: the more widely used Pederson−Khanna (PK) approach[28] as well as a recently derived linear response method that is referred to as coupled-perturbed SOC (CP-SOC) approach.[29] The spin−spin term in the DFT calculations[30] was obtained from the unrestricted natural orbital derived spin density as described by Sinnecker and Neese[31] without any further approximation. Calculations were carried out with the BP86 and B3LYP[32] functionals, which are good representatives of the class of generalized-gradient approximation and hybrid functionals, respectively.

For the CASSCF calculations, the SOC matrix was diagonalized in the basis of the 5 lowest quintet and 35 lowest triplet states. From the resulting magnetic sublevels, the D and E/D values are obtained from the matching procedure for d^4, $S = 2$, previously described.[33] In addition, a second-order perturbation value is obtained using the equations derived earlier.[34] Diagonalization of this second-order sum-over-states D tensor yielded the orientation of the D tensor in the molecular frame.

The prediction of the ZFS on the basis of first-principles electronic structure calculations faces several challenges: First, the calculations need to be based on an accurate structure.[35] This is particularly pressing for the calculation of the D tensor since the D value is zero for a system with cubic symmetry. Hence, at least to second order in perturbation theory, the entire ZFS effect arises from noncubic distortions in the ligand field. If optimized structures are used, their quality needs to be very high. However, even if the chosen method for geometry optimization is intrinsically accurate, it will usually not be sufficient to perform the optimizations in vacuum, since any contributions to the distortion arising from the crystal environment and the counterions will not be adequately taken into account by the calculations. Conversely, if experimental structures are available, their quality is also crucial for the success of the calculations. In particular, the positions of the hydrogen atoms are not usually defined to high precision if the structures are derived from X-ray diffraction experiments. The case of Jahn−Teller active systems may be considered as particularly challenging if the Jahn−Teller effect becomes dynamic and the uncertainties of the positions of the first ligand sphere are in doubt from experiments or may not be accurately predicted by the calculations that take no account of non-Born−Oppenheimer effects that prominently arise in Jahn−Teller systems.[36]

Second, even if an accurate structure is available, the demands on the electronic structure method for an accurate prediction of the ZFS are very high. This arises because the D tensor is composed of two leading microscopic interactions:[37] (a) the direct magnetic dipole−dipole interaction (to first order in perturbation theory) and (b) the spin−orbit coupling (to second order in perturbation theory). Both operators are complicated spin-dependent two-electron operators that are not easily handled in electronic structure theory. While it was believed for a long time that in transition-metal chemistry the SOC term is dominant, recent results suggest that this is not the case, at least not in general, and both interactions need to be considered.[33] Moreover, the second-order SOC term couples multiplets of different total spin.

In DFT, the accurate treatment of two-electron observables is an open problem and one usually has to rely on pragmatic approaches that assume correspondence between the true N-electron wavefunction and the Kohn−Sham determinant. However, even then the proper treatment of the spin-flip contributions to the SOC part of the D tensor is open to

(22) Neese, F. *ORCA−An ab Initio, Density Functional and Semiempirical Program Package*, version 2.6.03L; University of Bonn: Bonn, Germany.

(23) Schäfer, A.; Huber, C.; Ahlrichs, R. *J. Chem. Phys.* **1994**, *100*, 5829.

(24) Hess, B. A.; Marian, C. M.; Wahlgren, U.; Gropen, O. *Chem. Phys. Lett.* **1996**, *251*, 365. Berning, A.; Schweizer, M.; Werner, H. J.; Knowles, P. J.; Palmieri, P. *Mol. Phys.* **2000**, *98*, 1823.

(25) Neese, F. *J. Chem. Phys.* **2005**, *122*, 34107.

(26) Eichkorn, K.; Treutler, O.; Öhm, H.; Häser, M.; Ahlrichs, R. *Chem. Phys. Lett.* **1995**, *242*, 652. Eichkorn, K.; Weigend, F.; Treutler, O.; Ahlrichs, R. *Theor. Chem. Acc.* **1997**, *97*, 119. Eichkorn, K.; Treutler, O.; Öhm, H.; Häser, M.; Ahlrichs, R. *Chem. Phys. Lett.* **1995**, *240*, 283.

(27) Becke, A. D. *Phys. Rev. A: At., Mol., Opt. Phys.* **1988**, *38*, 3098. Perdew, J. P. *Phys. Rev. B: Condens. Matter Mater. Phys.* **1986**, *34*, 7406.

(28) Pederson, M. R.; Khanna, S. N. *Phys. Rev. B: Condens. Matter Mater. Phys.* **1999**, *60* (13), 9566.

(29) Neese, F. *J. Chem. Phys.* **2007**, *127*, 164112. For earlier discussions, see: Schöneboom, J.; Neese, F.; Thiel, W. *J. Am. Chem. Soc.* **2005**, *127*, 5840. Ray, K.; Begum, A.; Weyhermüller, T.; Piligkos, S.; van Slageren, J.; Neese, F.; Wieghardt, K., *J. Am. Chem. Soc.* **2005**, *127*, 4403.

(30) McWeeny, R.; Mizuno, Y. *Proc. Roy. Soc. London* **1961**, *A259*, 554. Petrenko, T. T.; Petrenko, T. L.; Bratus, V. Y. *J. Phys.: Condens. Matter* **2002**, *14*, 12433.

(31) Sinnecker, S.; Neese, F. *J. Phys. Chem. A* **2006**, *110*, 12267.

(32) Lee, C.; Yang, W.; Parr, R. G. *Phys. Rev. B: Condens. Matter Mater. Phys.* **1988**, *37*, 785. Becke, A. D. *J. Chem. Phys.* **1993**, *98*, 5648. Becke, A. D. *J. Chem. Phys.* **1993**, *98*, 1372. Stephens, P. J.; Devlin, F. J.; Chabalowski, C. F.; Frisch, M. J. *J. Phys. Chem.* **1994**, *98*, 11623.

(33) Neese, F. *J. Am. Chem. Soc.* **2006**, *128*, 10213.

(34) Neese, F.; Solomon, E. I. *Inorg. Chem.* **1998**, *37*, 6568.

(35) Zein S.; Duboc, C.; Lubitz, W.; Neese, F. *Inorg. Chem.*, submitted for publication.

(36) Bersuker, I. *The Jahn−Teller Effect*; Cambridge University Press: Cambridge, 2006.

(37) Harriman, J. E. *Theoretical Foundations of Electron Spin Resonance*; Academic Press: New York, 1978. For recent reviews, see: Neese, F.; Solomon, E. I. In *Magnetism: Molecules to Materials;* Miller, J. S., Drillon, M., Eds.; Wiley-VCH: Weinheim, Germany, 2002; Vol. IV, pp 345. Neese, F. Zero-field splitting. In *Calculation of NMR and EPR Parameters. Theory and Applications*; Kaupp, M., Bühl, M., Malkin, V. G., Eds.; Wiley-VCH: Weinheim, Germany, 2004. Neese, F. In *Mag. Res. Biol.*; Hanson, G., Ed., in press.

Table 5. Results of Electronic Structure Calculations on [Mn(bpia)(OAc)(OCH$_3$)]$^+$ Using a Variety of Different Theoretical Approaches and Structures. All Calculations Were Performed with the TZVP Basis Set

		experimental structure		hydrogen positions optimized		fully optimized structure	
		D	E/D	D	E/D	D	E/D
BP86	CP[a]	2.41	0.27	2.41	0.27	−2.19	0.32
BP86	PK[b]	2.12	0.28	2.11	0.28	−1.98	0.31
B3LYP	CP	2.77	0.26	2.76	0.26	2.77	0.26
B3LYP	PK	2.46	0.27	2.45	0.26	2.45	0.27
SA-CASSCF[c]		3.24	0.16	3.24	0.16	3.03	0.24

[a] CP = coupled-perturbed method proposed in ref 29. [b] PK = Pederson−Khanna method[28] with inclusion of the spin−spin term. [c] Contains only the SOC.

debate (for recent discussions, see refs 29, 33, 37, and 38). In this respect, multiconfigurational ab initio methods are more straightforward since all magnetic sublevels of all multiplets can be explicitly represented, and hence, their spin−orbit and spin−spin interactions can be computed without further assumptions.[39] Unfortunately, however, the demands on the quality of the basis set and the level of dynamic correlation treatment are so high in these methods that it becomes very difficult to apply them to systems such as the [Mn(bpia)(OAc)(OCH$_3$)]$^+$ complex with 50−60 atoms. Nevertheless, we have previously found[33] that ab initio calculations at the multiconfigurational entry level, using the CASSCF method, provide results for ZFSs that are fairly reasonable and usually superior to those predicted by DFT methods.

In order to have a well-defined active space with a clear connection to ligand field theory, it is advisable to confine the active space to MOs mainly of metal 3d character and to average the CASSCF solutions over the lowest multiplets. The diagonalization of the SOC operator in the basis of all d^N multiplets then represents no further computational challenge. It can reasonably be expected that this approach covers the leading SOC effects as long as the calculations do not grossly misrepresent the metal−ligand bonds. Thus, such calculations are expected to be acceptably successful if the metal−ligand bonds are predominantly ionic. It is bound to fail for covalent metal−ligand bonding, which will not be properly predicted by the CASSCF method with only metal-based orbitals in the active space.

Our results for the ZFS tensor of [Mn(bpia)(OAc)-(OCH$_3$)]$^+$ are collected in Table 5. Several conclusions arise:

The results obtained with the experimental structure are virtually indistinguishable from those where only the hydrogen atom positions were optimized but the results based on the optimized structure change noticeably. With the use of the BP86 DFT method, even the predicted sign of D changes and becomes inconsistent with experiment. In addition, the E/D values for this structure invariably become too rhombic for all electronic structure approaches. Thus,

as for the Mn(II) complexes discussed in ref 33, we conclude that the experimental structure is to be preferred for ZFS tensor calculations.

Comparison of the ab initio and DFT approaches shows that the former are more successful for the prediction of the ZFS tensor. While the state-averaged CASSCF values are in excellent agreement with the D value derived from the experimental analysis, the agreement is somewhat fortuitous since the spin−spin coupling has not been included in the CASSCF calculations reported in Table 4. We have separately calculated the spin−spin tensor in single-root CASSCF-(4,5) calculations with the result being a contribution to the D value of +1.3 cm^{-1} and a slight increase in the calculated rhombicity to $E/D = 0.21$. Thus, if done in a fully consistent manner, the calculations overestimate the D value by ∼25%, which is considered to be a fairly reasonable result given the simplicity of the approach. The overestimation should probably be attributed mainly to overly ionic metal−ligand bonding that leaves too much spin on the central manganese and hence leads to somewhat exaggerated SOC effects. The calculated rhombicity from the CASSCF calculations is also in excellent agreement with experiment. It is pleasing that the CASSCF values predicted by second-order perturbation theory ($D = 3.17$ cm^{-1} and $E/D = 0.16$) are in excellent agreement with the "infinite-order" results in Table 4. This result confirms that the fourth- (and higher-)order contributions to the spin-Hamiltonian are indeed small, as has already been inferred from the EPR experiments.

As found previously,[33] all DFT calculations significantly underestimate the D value and overestimate the E/D values. This is consistent with the typical quality of g tensor calculations in such systems (for reviews, see ref 37). Comparing the recently developed CP-SOC method[29] to the PK approach[28] reveals that the CP-SOC method is more successful, since it yields larger D values that are closer to experiment. This is mainly due to the revised prefactors for the spin-flip terms, as discussed previously.[29] Of the DFT methods, the best ZFS values are delivered by the B3LYP functional that underestimates the D value only slightly but still leads to an exaggerated E/D value. Again, such behavior is consistent with the experience gained in g-tensor calculations on transition-metal systems and argues in favor of the physical content of the CP-SOC approach.

The orientation of the ZFS tensor on the basis of the CASSCF calculations is shown in Figure 8. The z axis is closely aligned with the short Mn−O1 and Mn−N2 bond vectors, as expected. The calculated direction of D_{xx} is in close agreement with that calculated using the AOM for the model complex, lying close to the Mn−N1 bond, suggesting that the x axis is determined largely by the angular distortion.

Comparison of the experimental and optimized structures (Figure 9) reveals that the optimizations, despite having been performed with a reasonably large basis set, show some rather large errors. While the metal−ligand distances for the anionic ligands are predicted with acceptable accuracy (deviations are 2−4 pm), the distances to the neutral imidazole and amine ligands are significantly overestimated by up to 10 pm in the calculations. Hence, the equatorial

(38) Reviakine, R.; Arbuznikov, A.; Tremblay, J.-C.; Remenyi, C.; Malkina, O. L.; Malkin, V. G.; Kaupp, M. *J. Chem. Phys.* **2006**, *125*, 054110. Neese F.; Petrenko, T.; Ganyushin, D.; Olbrich, G. *Coord. Chem. Rev.* **2007**, *205*, 288.
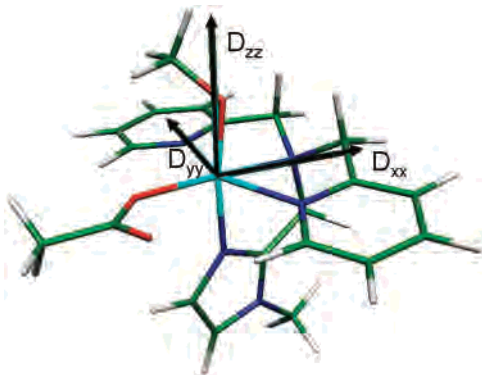(39) Neese, F.; Petrenko, T.; Ganyushin, D.; Olbrich, G. *Coord. Chem. Rev.* **2007**, *205*, 288.

Figure 8. Orientation of the *D* tensor in the molecular coordinate system according to state-averaged CASSCF(4,5) results with the TZVP basis set.
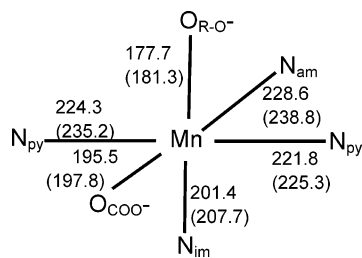

Figure 9. Comparison of experimental[6] and RI-BP86/TZVP-optimized (in brackets) metal−ligand distances (in pm).

ligand field becomes too weak in the computations. Second, since the carboxylate ligand is in the equatorial plane, the differences between D_{xx} and D_{yy} are exaggerated in the calculations based on the optimized structure, and hence, the predicted rhombicity becomes too large.

5. Summary and Conclusions

In this work, spectroscopic data for [Mn(bpia)(OAc)-(OCH$_3$)](PF$_6$) have been presented, affording the determination of the $S = 2$ ground-state spin-Hamiltonian parameters to fourth order in the ZFS terms. The energy separations between the low-lying states span a range particularly favorable for the application of INS. Good-quality spectra have been obtained without the need for deuteration, proving the worth of the technique for the study of bioinorganic transition-metal compounds. To our knowledge, this is the first instance where the spin-Hamiltonian parameters of a system have been determined by the concomitant analysis of EPR and INS data.

The heteroleptic coordination and pronounced angular distortion of the first coordination sphere are typical of monomeric manganese(III) systems in biology, which, as we have stated, are often more amenable to spectroscopic probes than to crystallographic determinations. The positive value of *D* that has been determined demonstrates that the correlation between the sign of the *D* parameter and the nature of the Jahn−Teller distortion still persists when the angular distortion of the first coordination sphere is acute, a result supported by elementary AOM calculations, i.e., the ZFS parameters remain a reliable guide as to whether the complex is tetragonally compressed or elongated.

In addition to this generalization, the electronic structure calculations presented reveal the extent to which the electronic and molecular structure may be interrelated for compounds of this complexity. Attempts to reproduce the ZFS parameters by electronic structure calculations are instructive by both their promise and shortcomings. Those calculated by CASSCF calculations are astonishingly close to the experimental values if the spin−spin coupling contribution is discarded. This result comes on the back of the calculation of the ZFS parameters for the [Mn(acac)$_3$] complex, by the same method, that shows an equally satisfactory semblance to the experimental values.[33] However, inclusion of the substantial spin−spin term of +1.3 cm^{-1} worsens the agreement with experiment somewhat. Nevertheless, we feel that these calculations provide a realistic microscopic approach to the problem of ZFSs in Mn(III) complexes. To improve substantially upon these results would require the treatment of electron correlation effects to much higher sophistication, which remains a very laborious task for molecules of the present size.

Conversely, while being in qualitative accord with experiment, the DFT approaches fail to provide an accurate prediction of the experimental structure and overestimate the rhombic contribution to the anisotropy of the *D* tensor. The results emphasize the need for molecules of this complexity to be studied by a range of experimental and theoretical techniques. Over reliance on DFT could lead to false deductions concerning the structure and bonding. The question as to why a tetragonally compressed geometry is favored over the more commonly observed elongation is the subject of the next paper.